Simulation of the Tianwen-4 Mission Contribution to Jupiter Gravity Field Improvement

Afzal, Zohaib; Yan, Jianguo; Dirkx, Dominic; Huang, Yong; Wang, Zhen; Haider, Zeeshan; Barriot, Jean Pierre

DOI
10.3847/1538-4357/adb1e8

Publication date
2025

Document Version
Final published version

Published in
Astrophysical Journal

Citation (APA)
Afzal, Z., Yan, J., Dirkx, D., Huang, Y., Wang, Z., Haider, Z., & Barriot, J. P. (2025). Simulation of the Tianwen-4 Mission Contribution to Jupiter Gravity Field Improvement. *Astrophysical Journal*, *981*(2), Article 163. https://doi.org/10.3847/1538-4357/adb1e8

The Astrophysical Journal, 981:163 (15pp), 2025 March 10 https://doi.org/10.3847/1538-4357/adb1e8

Simulation of the Tianwen-4 Mission Contribution to Jupiter Gravity Field Improvement

Zohaib Afzal[1], Jianguo Yan[1,2], Dominic Dirkx[3], Yong Huang[4], Zhen Wang[2], Zeeshan Haider[1], and Jean-Pierre Barriot[1]
[1] State Key Laboratory of Information Engineering in Surveying, Mapping and Remote Sensing, Wuhan University, Wuhan, People's Republic of China; jgyan@whu.edu.cn
[2] Xinjiang Astronomical Observatory, Chinese Academy of Sciences, Urumqi 830011, People's Republic of China
[3] Delft University of Technology, Kluyverweg 1, 2629HS, Delft, The Netherlands
[4] Shanghai Astronomical Observatory, Shanghai 200030, People's Republic of China
Received 2024 October 9; revised 2025 January 14; accepted 2025 January 21; published 2025 March 6

Abstract

This study comprehensively evaluates the impact of the expected Chinese Tianwen-4 mission, in conjunction with the existing data from the Juno mission, on enhancing the understanding of Jupiter's gravity field. Integrating simulated data from both missions. The methodology incorporates detailed simulations of Tianwen-4's orbit, assessing its influence on Jupiter's gravity field estimations across various orbital inclinations. It also explores the integration of multimission tracking data, combining simulated Juno and Tianwen-4 data. In addition to the static gravity coefficient, the analysis extends to include the tidal effect k_{nm}, which quantifies the tidal response of Jupiter's gravity field to forcing it by the Galilean satellites. The results indicate clear potential improvements in the precision of the gravity field models compared to those derived from the Juno mission alone, particularly in the lower degree harmonics, where accuracy improves by an average factor of 20.08 in the first 12°, gradually decreasing to 2.46, with an overall enhancement of 7.43. These enhancements underscore the value of integrating data from multiple missions, which provides a more nuanced understanding of Jupiter's gravitational properties. Improving the gravity field model is essential for gaining deeper insights into Jupiter's internal structure and dynamics, which ultimately enhances our understanding of giant planets and their formation. Accurate gravity models are crucial for interpreting a planet's physical and chemical properties, leading to better comprehension of planetary systems.

Unified Astronomy Thesaurus concepts: Gravitational fields (667); Orbit determination (1175); Solid body tides (2298); Jupiter (873); Jovian satellites (872); Natural satellites (Solar system) (1089)

Materials only available in the online version of record: data behind figures

1. Introduction

Exploring Jupiter's gravity field is crucial for comprehending the distribution of mass within the planet, shedding light on its internal composition and dynamic activities (T. Guillot et al. 2004). Given the challenges associated with in situ exploration, the primary method for studying Jupiter involves analyzing combined data sets from gravity measurements and atmospheric dynamics (Y. Kaspi et al. 2010), which are crucial for understanding its formation and evolution within our solar system. Improving Jupiter's gravity field models is crucial for advancing our knowledge of the gas giant's underlying physical and chemical processes, and it also supports the accurate navigation of spacecraft during Jovian missions (S. J. Bolton et al. 2021).

Launched in 2011 and reaching Jupiter in 2016, the Juno mission has been orbiting the planet, delivering crucial data via its array of nine instruments. A primary objective of Juno's mission centers on Jupiter's radio science investigation (S. W. Asmar et al. 2017). This involves measuring the Doppler shifts in microwave signals transmitted between Earth and the spacecraft, which facilitates detailed assessments of Jupiter's internal mass distribution, core structure, and rotational dynamics (D. J. Stevenson 2020).

Jupiter's atmosphere features marked east–west zonal jet streams that play a significant role in creating the planet's characteristic red and white bands (A. R. Vasavada & A. P. Showman 2005). Each hemisphere contains six pairs of jet streams. On the equatorial side of these jets, there is an eastward current moving at approximately 100 m s^{-1} with respect to the System III reference frame, exhibiting super-rotation close to the equator within 6° (Y. Kaspi et al. 2009). Beyond 65° latitude toward the poles, the jet streams give way to a dynamic dominated by vortices extending to the polar regions. Jupiter's winds shape its gravitational field by altering density distributions, which are then captured in the planet's gravity model coefficients.

Early results from the Juno mission included identifying a north–south imbalance in Jupiter's gravitational field (L. Iess et al. 2018). This imbalance is associated with comparable variations found in the wind patterns at the cloud level of Jupiter (Y. Kaspi et al. 2018) and aligns with pre-Juno predictions regarding the gravitational effects of varying flow depths (Y. Kaspi 2013). This understanding primarily emerged from studying odd gravity harmonics J_3, J_5, J_7, and J_9 and was further supported by aligning low-degree even harmonics J_6, J_8, and J_{10} after making adjustments for contributions from internal densities (T. Guillot et al. 2018).

The gravity harmonic coefficients J_n provide valuable insights into the distribution of planetary density when projected onto a Legendre polynomial basis function. Traditionally, these coefficients are typically used to represent the gravity fields of almost spherical celestial objects (T. Guillot 1999; S. M. Wahl

et al. 2017). The accurate gravity measurements carried out by the Juno mission have enabled the detection of minor variations in Jupiter's gravity field (W. M. Folkner et al. 2017; M. Parisi et al. 2021). These variations are linked to planetary flows that create a geostrophic density anomaly, which in turn affects the gravity signal detected by the mission (Y. Kaspi et al. 2010).

As a result, Jupiter's density can be separated into two parts: a static component, which is symmetrical across the north and south because there are no hemispherical differences in the average radial density profile, and a dynamic component resulting from planetary flows. This dynamic component contributes to both symmetric and asymmetric elements (Y. Kaspi 2013). The static part of the gravity harmonics diminishes quickly with higher degrees, whereas the dynamic component maintains a similar magnitude across higher harmonics, influenced by the latitudinal variations in wind-induced density changes (W. B. Hubbard 1999). Notably, the gravity signal for harmonics beyond J_{10}, including both even and odd high-degree terms, is entirely attributable to dynamic factors.

The precise measurements of Jupiter's gravity field obtained by the Juno spacecraft using dual-frequency Doppler tracking at *X*-band and *Ka*-band have revealed unexpected time-variable components in the gravitational field. These anomalies could not be solely attributed to the static field or localized density anomalies. One plausible explanation for these anomalies is the presence of normal modes of internal oscillations within Jupiter that propagate outward and cause periodic variations in its gravity field. These normal modes were detected in the Doppler data, indicating perturbations on the spacecraft with amplitudes ranging from 2 to 5×10^{-8} m s^{-2}. The observed anomalies, with peak radial velocities of 10–50 cm s^{-1} at frequencies between 900 and 1200 μHz, suggest significant internal oscillations that propagate to Jupiter's surface that affect the gravitational field's symmetry. The complexity and variability of these modes necessitate a flexible approach to account for their influence on the gravity field accurately (D. Durante et al. 2022).

In earlier research (W. M. Folkner et al. 2017; L. Iess et al. 2018; D. Durante et al. 2020), gravity measurements were able to discern individual harmonics up to $\boldsymbol{J_{10}}$, allowing for the evaluation of flow depths through the use of low-degree odd harmonics $\boldsymbol{J_3}$, $\boldsymbol{J_5}$, $\boldsymbol{J_7}$, and $\boldsymbol{J_9}$ or by extracting the static part of the even harmonics J_6–J_{10} based on models of Jupiter's internal structure (T. Guillot et al. 2018). J_{10} marks the transition where Jupiter's gravity spectrum shifts from atmospheric to internal dynamics, influencing both even and odd harmonics. This convergence allows for a precise determination of the dynamical influences on Jupiter's gravity field.

Recent research has broadened the analysis to include higher degree harmonics, reaching up to J_{40}. This expansion has yielded vital insights into the influence of Jupiter's cylindrical flow orientations on its gravity harmonics and the resulting wavy patterns in gravity signals. The increase to J_{40} was facilitated by applying spatial constraints at high latitudes, allowing the gravity harmonics to be resolved up to this higher degree. Such advanced analysis has been crucial for linking observable cloud-level winds to deeper atmospheric structures, demonstrating the significant impact of cylindrical flows on the subtleties of the planet's gravitational field (Y. Kaspi et al. 2023).

The tidal effects of Jupiter due to gravitational forces from its moons are measured using tidal Love numbers (A. E. H. Love 1911), which are vital for understanding the deep internal structure of Jupiter. According to studies by L. Iess et al. (2018), V. Notaro et al. (2019), and S. M. Wahl et al. (2016), these quantities provide essential insights into the internal composition and dynamics of the planet. The orbital configuration of the Juno spacecraft, as well as the positioning of the Jovian moons, plays a vital role in accurately determining the satellite-dependent tidal effects on Jupiter.

To accurately measure the tidal bulge of Jupiter induced by a particular moon, it is crucial that the longitudes of that moon are evenly distributed over the different gravity-centric pericenter passes of Juno. This ensures that the tidal effects are sampled comprehensively over time. The tidal bulge induced by Io on Jupiter is uniformly distributed in longitude, enabling comprehensive sampling of its effects. Juno's trajectory provides adequate longitudinal coverage for tidal interactions involving Io, Europa, and Ganymede, but it is less effective for Callisto due to the mission's limited time span. Although Juno's orbital period is nearly resonant with Io, which is in a 4:2:1 Laplace resonance with Europa and Ganymede (J. Fuller et al. 2016), This enhances the accuracy and reliability of tidal data collected by Juno, providing a robust framework for studying Jupiter's gravitational interactions with its moons.

Tianwen-4 is a proposed Chinese space mission that aims to explore Jupiter, the largest planet in the solar system and its moon Callisto. Scheduled for a launch in 2029 September, Tianwen-4 represents China's ambitious endeavor to study the gas giant and its environment (S. Sun et al. 2024). The mission anticipates involving a number of spacecraft, with the goal of being captured by Jupiter by 2035 December. Building on China's successful missions like Tianwen-1 (S. Shangbiao et al. 2025), which achieved orbit insertion around Mars in 2021 February, and the Chang'e lunar exploration missions, Tianwen-4 is set to advance our knowledge of the solar system. In addition to investigating Jupiter's atmosphere, magnetosphere, and moons, the mission objectives will include conducting gravity field experiments to enhance our understanding of Jupiter's complex gravitational system, providing critical insights into its internal dynamics, and advancing our knowledge of planetary formation and behavior in nature.

Building on these substantial observational and theoretical advancements, this paper aims to evaluate the potential improvements in the accuracy of spherical harmonic coefficients up to J_{40}. By leveraging anticipated data from the future Chinese Tianwen-4 mission to Jupiter, this study proposes a dynamic methodology to enhance the precision of these order and degree coefficients, thereby contributing significantly to the broader discourse on planetary formation and atmospheric science within our solar system.

The paper is structured as follows: Section 2 outlines the theoretical framework, including mathematical models relevant to Jupiter's gravitational dynamics. Section 3 details the methodology, such as the simulation setup and data sources. In Section 4, we analyze the simulation results and their significance for planetary science. Section 5 summarizes the findings.

2. Theoretical Framework

2.1. Covariance Analysis

To assess the potential improvements in the estimation accuracy of Jupiter's interior properties, we performed several covariance analyses across various scenarios. The covariance matrix $\boldsymbol{P}$ of the estimated parameters is determined using the

method outlined by O. Montenbruck et al. (2002).

$$\boldsymbol{P} = (\boldsymbol{H}^T\boldsymbol{W}\boldsymbol{H} + \boldsymbol{P}_0^{-1})^{-1}. \quad (1)$$

In this context, $\boldsymbol{W}$ is the observation weight matrix, and $\boldsymbol{H}$ is the partial derivative matrix relating observations to parameters. The matrix $\boldsymbol{P}_0$ reflects our a priori covariances before estimation, while the accuracy of the estimation is represented by the covariance matrix $\boldsymbol{P}_c$, defined as follows:

$$\boldsymbol{P}_c = \boldsymbol{P} + (\boldsymbol{P}\boldsymbol{H}^T\boldsymbol{W})(\boldsymbol{H}_c\boldsymbol{C}\boldsymbol{H}_c^T)(\boldsymbol{P}\boldsymbol{H}^T\boldsymbol{W})^T. \quad (2)$$

The matrices $\boldsymbol{P}$, $\boldsymbol{H}$, and $\boldsymbol{W}$ are as defined in Equation (2). Here, $\boldsymbol{H}_c$ represents the observation of partial derivatives related to the considered parameters, and $\boldsymbol{C}$ is the covariance matrix reflecting our knowledge of these parameters. The formal uncertainties of the estimated parameters are calculated as the square root of the diagonal elements of $\boldsymbol{P}$ and $\boldsymbol{P}_c$. These formal errors can be propagated to any epoch t using the following method:

$$\boldsymbol{P}(t) = [\boldsymbol{\Phi}(t, t_0)\,\boldsymbol{S}(t)]\boldsymbol{P}[\boldsymbol{\Phi}(t, t_0)\,\boldsymbol{S}(t)]^T. \quad (3)$$

In this context, $\boldsymbol{\Phi}(t, t_0)$ represents the state transition matrix, and $\boldsymbol{S}(t)$ denotes the sensitivity matrix. The same equation can propagate the considered covariance matrix $\boldsymbol{P}_c$ instead of $\boldsymbol{P}$. The $\boldsymbol{P}$ on the left-hand side is the propagated covariance of the state only, while the $\boldsymbol{P}$ in the middle represents the full covariance of all parameters.

2.2. Jupiter Spherical Harmonic Gravity

The gravitational potential of a celestial body can be described through a series of spherical harmonic basis functions $Y_{nm}(\theta, \varphi)$. They provide functions on the unit sphere on an orthonormal basis; they are individually identified by their degree (n) and order (m). These series are modified by a scaling factor that depends on the normalized radial distance r/R from the body's center, where R represents the equatorial radius. This formulation enables a global representation of the body's gravitational field relative to positions on and surrounding the body (B. Bertotti et al. 2003).

$$U(r, \theta, \varphi) = \frac{GM}{r}\left[1 + \sum_{n=2}^{\infty}\left(\frac{R}{r}\right)^n \sum_{m=0}^{n} U_{nm}Y_{nm}(\theta, \varphi)\right]. \quad (4)$$

Here, GM stands for the gravitational parameter, which is the result of multiplying the planet's mass M by the gravitational constant G. The radius R used in these calculations is typically the equatorial radius of the planet, reflecting the circumscribing sphere of bodies that are not perfect spheres due to rotational flattening. If the internal density distribution ρ of the planet were precisely determined, the harmonic coefficients U_{nm} could be calculated by performing an integration across the planet's volume V.

$$U_{nm} = \frac{1}{(2n+1)MR^n}\int_V (r')^n Y_{nm}^*(\theta', \varphi')\rho(r', \theta', \varphi')dV'. \quad (5)$$

In cases where the density is uniform across longitudes, as is typical for a fluid and fast-spinning planet like Jupiter (L. Iess et al. 2018), the corresponding expression can be simplified as:

$$U_{n0} = \frac{1}{MR^n}\int_V (r')^n P_n(\theta')\rho(r', \theta')dV' \quad (6)$$

$$J_n = \sqrt{2n+1}\; U_{n0}. \quad (7)$$

P_n here stands for the Legendre polynomial of degree n. Thus, the zonal coefficients J_n provide important insights into Jupiter's interior density distribution, though this information is not unique.

2.3. Gravity Field Variation due to Tides

The gravitational potential of Jupiter, perturbed by tidal forces, can be expressed as being proportional to the perturbing potential, mediated through the Love numbers k_{nm} (A. E. H. Love 1911). Consequently, the effect of tides on Jupiter's gravity field can be expressed as a change in the spherical harmonic coefficients of the gravity field (T. D. Moyer 2003).

$$\Delta\bar{J}_n = \frac{-1}{2n+1}k_{n0}\sum_j \frac{GM_j}{GM_\oplus}\left(\frac{R}{r_j}\right)^{n+1}\bar{P}_{n0}(u_j), \quad (8)$$

$$\Delta\bar{C}_{nm} - i\Delta\bar{S}_{nm} = \frac{1}{2n+1}k_{nm}\sum_j \frac{GM_j}{GM_\oplus}\left(\frac{R}{r_j}\right)^{n+1} \times\bar{P}_{nm}(u_j)(s_j - it_j)^m.$$

In Equation (8), $\bar{C}_{nm}$ and $\bar{S}_{nm}$ are the fully normalized spherical harmonic coefficients of degree n and order m. $GM_\oplus$ represents the gravitational parameter of Jupiter, while GM_j denotes the gravitational parameter of the jth satellite. The variable r_j indicates the radial distance from Jupiter to the jth satellite. Additionally, s_j, t_j, and u_j are the three Cartesian components of the unit vector fixed in Jupiter's body frame, pointing toward the jth perturbing satellite.

3. Methodology

In this section, we outline the methodologies employed to assess the effects of the Tianwen-4 mission's orbital dynamics on the gravitational field solutions for Jupiter. Our approach integrates numerical simulations with modeled orbital dynamics to analyze and compare the outcomes with those derived from the Juno mission. We detail the simulation scenarios, data acquisition methods, and analytical techniques used to interpret the gravity field coefficients. This ensures a comprehensive understanding of how orbital variations influence the accuracy and reliability of gravitational measurements.

3.1. Description of Simulation

In this study, we evaluated the impact of the Tianwen-4 orbit on the solution of the gravity field for Jupiter. Specifically, the inclination of the Tianwen-4 orbit has been adjusted for simulation, as detailed in Table 1. We have developed two simulation scenarios, one based on the Juno mission reference trajectory, providing a well-established baseline for comparison and validation, and another exploring various potential orbital configurations for the future Tianwen-4 mission, with a focus on different orbital inclinations. In these situations, the solutions are formed by applying the initial orbital elements. Furthermore, we examined two different orbital inclinations in the Tianwen-4 scenario to show how variations in inclination affect the precision of the solution for Jupiter's gravity field. According to personal communication, the possible inclination of the Tianwen-4 spacecraft is around 40°, thus we chose this inclination in our simulation. As polar orbit is a popular setting

Table 1
The Tianwen-4 Orbital Elements Used in the Simulation

Parameter	Value
Semimajor axis (m)	2827706000
Eccentricity	0.9733
Inclination (degree)	40, 90
RAAN (degree)	321.2
Argument of perigee (degree)	355.1

for Jupiter exploration as it provides comprehensive coverage of Jupiter's latitudes. We also include an inclination of 90° for a bench test, which is another potential configuration for the Tianwen-4 mission. This analysis takes into account multiple aspects, such as the gravity field coefficients' formal uncertainties, their intercorrelation, the accuracy of orbit determination, the calculation of the k_{lm} Love Number, and the error distribution.

Figures 1 and 2 present comparative visualizations of the Tianwen-4 spacecraft's ground tracks over Jupiter. Figure 1 displays the ground tracks for a 40° equatorial orbit, while Figure 2 depicts those for a 90° polar orbit, both shown for the 12 month and 24 month mission durations.

Figure 1 illustrates the ground tracks of the Tianwen-4 spacecraft, focusing on its coverage of Jupiter's surface. Panel (a) depicts Tianwen-4's ground track with a 40° inclination, using 12 months of data over 10 hr periods of arc. This view provides insight into the spacecraft's coverage during its first year of operation. Panel (b) shows Tianwen-4's ground track, also with a 40° inclination, but using 24 months of data over 10 hr periods of arc. This panel demonstrates the enhanced coverage achieved with an extended mission duration. Both panels primarily focus on the equatorial region, allowing for a direct comparison of how mission duration affects the spatial distribution of observations. This visualization is crucial for understanding the impact of extended data collection on the comprehensive mapping of Jupiter's gravitational field, particularly in the equatorial zone.

Figure 2 illustrates the ground tracks of the Tianwen-4 spacecraft, showcasing its coverage of Jupiter's surface at a polar orbit. Panel (a) depicts Tianwen-4's ground track with a 90° inclination, using 12 months of data over 10 hr periods of arc. This view demonstrates the spacecraft's comprehensive latitudinal coverage during its first year of operation. Panel (b) shows Tianwen-4's ground track, also with a 90° inclination, but using 24 months of data over 10 hr periods of arc. This panel highlights the enhanced global coverage achieved with an extended mission duration, emphasizing the spacecraft's ability to map Jupiter's gravitational field across all latitudes. The comparison between these two panels illustrates the significant improvement in spatial distribution and density of observations that can be achieved by extending the mission duration in a polar orbit configuration. This enhanced coverage is also reflected in the correlations diagram (Section 4.3). Further expanding on Tianwen-4's observational capabilities, Figure 3 displays the orbit of the Tianwen-4 spacecraft around Jupiter.

In Figure 3, both Jupiter and the Tianwen-4 spacecraft's orbit are plotted in the X–Y plane. Jupiter is represented by a red circle at the center. The Tianwen-4 propagated orbit, spanning 3 yr, is displayed as blue lines around Jupiter. We account for the shifts in orbital parameters after each orbit caused by the complete set of gravitational harmonics. This layout illustrates a possible 40° mission configuration,

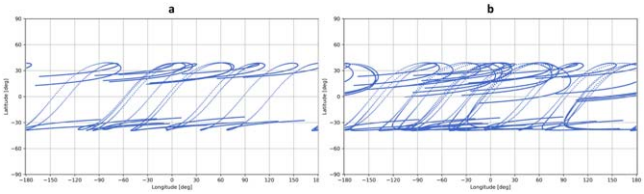

Figure 1. Satellite ground tracks visualized across two panels: (a) Tianwen-4 ground track with a 40° inclination using 12 months of data; (b) Tianwen-4 ground track with a 40° inclination using 24 months of data.

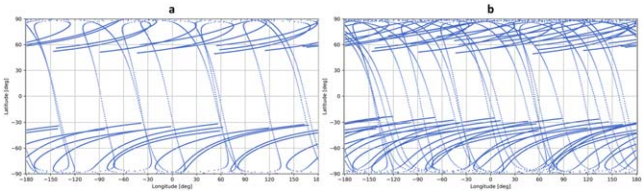

Figure 2. Satellite ground tracks visualized across two panels: (a) Tianwen-4 ground track with a 90° inclination using 12 months of data; (b) Tianwen-4 ground track with a 90° inclination using 24 months of data.

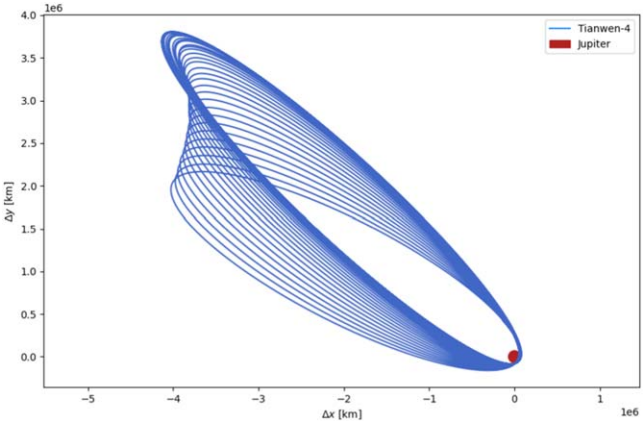

Figure 3. Tianwen-4 spacecraft's orbit around Jupiter, shown in a 40° possible mission configuration with a 3 yr orbital period.

highlighting the spacecraft's trajectory and its observational coverage of Jupiter's gravitational and atmospheric features.

In this study, satellite observations were simulated by terrestrial ground stations. For the Juno mission, we used facilities from NASA's Deep Space Network (DSN) located in Goldstone (United States) (S. D. Slobin 2016). For the Tianwen-4 mission, the tracking involved stations from the Chinese Deep Space Network (CDSN) in Kashi (China), Jiamusi (China), and Neuquén (Argentina) (J. Yan et al. 2017). The coordinates of all these stations can be found in Table 2. We employed two viability configurations in our analysis. In Tianwen-4 cases, we set the ground station elevation angle to a minimum of 10°. Additionally, for both Juno and Tianwen-4, we considered Jupiter as an occultation body, accounting for periods when the planet obstructs the line of sight between the spacecraft and Earth. Furthermore, we also removed any overlaps between the ground station visibility periods to ensure independent tracking.

To explore the potential contributions of radio tracking data from upcoming Chinese Jupiter missions and to assess its integration with data from previous Juno missions in studying Jupiter's gravity field, we conducted numerical simulations of gravity experiments using the TU Delft Astrodynamics

Table 2
Geodetic Positions of the Ground Stations Used in the Simulation

Station	Latitude	Longitude
NASA Deep Space Network		
Goldstone (United States)	35.1562591	243.1246368
Chinese Deep Space Network		
Jiamusi (China)	46.493403	130.770409
Kashi (China)	38.423420	76.712207
Neuquén (Argentina)	−38.191439	−70.149627

Toolbox (D. Dirkx et al. 2019, 2022), which has been used for simulated and real analyses of radio science solutions of planetary missions, such as evaluating ephemerides solution for the ESA's JUICE mission (S. Bauer et al. 2016; M. Fayolle et al. 2023, 2024). For the examination of the simulated data, our study encompasses data from two key missions to Jupiter: NASA's Juno and the future Chinese Tianwen-4 mission. For both missions, we evaluated the gravity field based on propagating initial conditions across 26 mission arcs of Juno, providing a consistent baseline for comparison. Juno's data collection began on 2016 August 27 (perijove 1) and continued through 2021 October 17 (perijove 37), offering an extensive data set for analysis. We limited our analysis to 26 mission arcs to align with the reference Juno solution, ensuring consistent uncertainty levels without introducing additional uncertainties (Y. Kaspi et al. 2023). To model Juno's trajectory, we propagated it over 7 hr arcs centered on each perijove, utilizing the most recent reference trajectory provided by NASA Navigation and Ancillary Information Facility (C. H. Acton et al. 1996).

The Tianwen-4 mission, scheduled to launch in 2030, presents an opportunity for future comparative analysis. For this upcoming mission, we simulated both 1 yr and 2 yr data sets starting from 2037 April. The spacecraft's trajectory was modeled using 10 hr arcs centered on the pericenter, allowing for a comprehensive comparison with Juno's observations. For Tianwen-4, extended arc periods were enabled by dual-frequency tracking from three ground stations, improving constraints and reducing overparameterization risk.

For both spacecraft, we utilized tracking data comprising two-way range rate measurements using *Ka* and *X*-band frequencies. The Juno mission included 26 arcs, with 19 arcs configured for dual-frequency observations and seven arcs for single-frequency observations (Y. Kaspi et al. 2023; Planetary Atmospheres Node 2024). In contrast, the Tianwen-4 mission included either 12 or 24 arcs, based on the scenario outlined in Section 3.1, all configured for dual-frequency observations to ensure a consistent data set for analysis. To these simulated observables, we applied random Gaussian white noise with standard deviations of 12.9 μm s^{-1} for the *Ka*-band and 22.5 μm s^{-1} for the *X*-band. Each measurement was integrated over a 60 s period to balance data resolution and noise reduction (L. Iess et al. 2018).

3.2. Estimation Methodology

The Doppler data from each observation arc are organized into a multiarc integration for covariance analysis (see Section 2.1). In this setup, the data from each arc contribute to the global parameters, such as Jupiter's gravity field and tidal reactions, as well as for local parameters specific to each arc, like Juno's position and velocity. This approach is particularly vital for addressing the significant errors that accumulate over Juno's 52.9 day and Tianwen-4's 30.73 day orbit caused by the extended periods between successive pericenter passes. By utilizing a multiarc strategy, we can effectively prevent dynamical model errors from accumulating, ensuring that the gravitational measurements remain accurate over longer observational periods (D. Serra et al. 2018). This method enhances the reliability of our data and improves the overall precision of the gravity field solutions.

Additionally, Doppler observables are calculated by solving the relativistic light-time equation. While Jupiter's oblateness is considered in the spacecraft's orbital modeling, it is not directly included in the relativistic light-time correction. For analysis of Doppler data, akin to the Tianwen-4 mission's methodology, this approach ensures the most accurate gravitational measurements by refining the spacecraft's tracked orbit based on the residual alignment with noise specifications.

3.3. Dynamical Models

The dynamical models for Juno incorporate various significant effects that influence the spacecraft's motion around Jupiter. This model integrates gravitational accelerations within a relativistic framework, accounting for the point mass gravity of solar system planets and Jupiter's Galilean moons. It characterizes Jupiter's oblate gravitational field using spherical harmonics and accounts for the gravitational variations due to solid body tides raised by the Jovian moons. The model incorporates Jupiter's rapid rotation, shifts in Jupiter's spin axis, and the synchronous rotation of its moons. Solar radiation pressure effects are modeled using a cannonball approach for both the Juno and Tianwen-4 spacecraft, with a reference area of 77.46 m^2, consistent with Juno's configuration (S. J. Bolton et al. 2017). For the ephemerides of planets and satellites, we employ JPL's DE440 for planetary data and for the moons of Jupiter (R. S. Park et al. 2021). The dynamical models include Jupiter's gravity field up to degree 40 (from J_2 to J_{40}) and the tesseral coefficients C_{21}, C_{22}, S_{21}, and S_{22}. The baseline values for the zonal gravity field coefficients are based on the latest calculations (Y. Kaspi et al. 2023).

We define the pole position of Jupiter by its R.A. α and decl. δ at a reference epoch in the IAU-defined reference frame for Jupiter. The orientation of Jupiter's body-fixed frame (IAU) relative to the inertial frame (I) at the reference epoch is represented by the following rotation matrix:

$$\boldsymbol{R}^{(\mathrm{IAU}/I)}(t_0) = \boldsymbol{R}_z(W_0)\boldsymbol{R}_x(\pi/2 - \delta)\boldsymbol{R}_z(\pi/2 + \alpha), \quad (9)$$

where W_0 is the prime meridian angle, δ is the decl. of the rotation axis, and α is the R.A. of the rotation axis. The term $\boldsymbol{R}_z(W_0)$ rotates the frame to align with the prime meridian, $\boldsymbol{R}_x(\pi/2 - \delta)$ adjusts the decl., and $\boldsymbol{R}_z(\pi/2 + \alpha)$ accounts for the R.A. of the pole. Together, this matrix describes the fixed orientation of Jupiter's rotation axis in the IAU-defined body-fixed frame. The continuous rotation of Jupiter about its z-axis over time is then described by the full transformation from the inertial frame (I) to the IAU-defined body-fixed frame (IAU):

$$\boldsymbol{R}^{(\mathrm{IAU}/I)}(t) = \boldsymbol{R}_z(\omega(t - t_0))\boldsymbol{R}^{(\mathrm{IAU}/I)}(t_0), \quad (10)$$

where ω is the constant rotation rate (rad s^{-1}), and t_0 is the reference epoch. This equation combines the fixed orientation

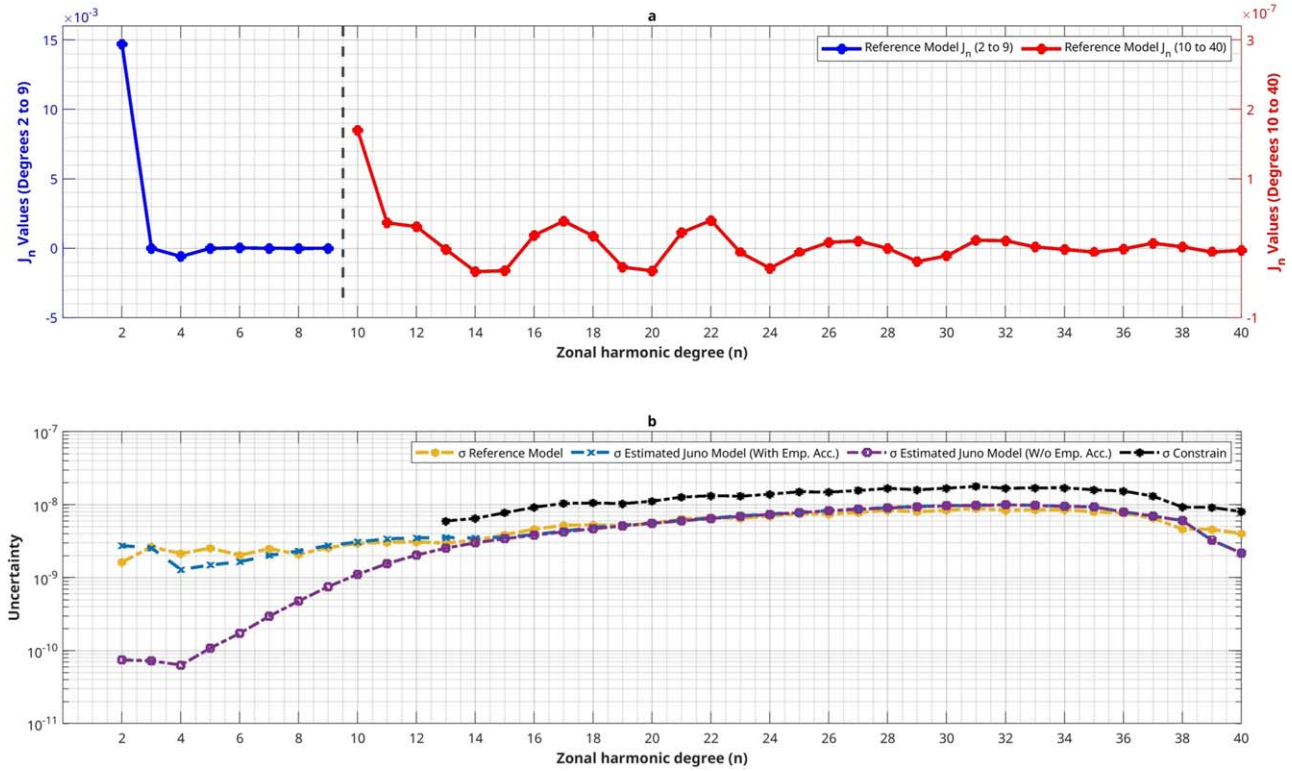

Figure 4. Formal uncertainties (σ) for the estimated Juno model. Panel (a) displays the zonal harmonics J_n, while panel (b) provides a comparative analysis of formal uncertainties on a logarithmic scale. The plot presents formal uncertainties (σ) for gravity field solutions derived from both the estimated Juno model and the reference model, comparing results with and without the inclusion of empirical accelerations, and includes the constraint applied from J_{13} to J_{40}.
(The data used to create this figure are available in the online article.)

of Jupiter's body at the reference epoch with its uniform rotation about the z-axis, ensuring consistency in the IAU-defined frame.

We selected this model because the Juno-only simulation accurately matches real Juno results without unnecessary complexities. A fully dynamical model, such as G. Lari et al. (2024), or variations in the reference pole, while valuable for other contexts, are less relevant to the specific focus of our study on gravitational field measurements. As shown in Figure 4, even without including pole rates, our Juno-only simulation aligns well with the actual Juno results, demonstrating that the simplified model achieves the required accuracy for our objectives.

The Juno spacecraft's gravity measurements have provided evidence for normal modes of Jupiter, observed as unexplained accelerations in the Doppler signal. These accelerations could not be attributed to localized density anomalies or nonaxisymmetric components of the static gravity field. Instead, internal oscillations within Jupiter, or normal modes, account for these time-variable gravitational features. Including these normal modes is crucial for better data fitting and robustness of the gravity field estimation. This enhancement provides a more reliable basis for interpreting Jupiter's overall gravitational characteristics. To address unexplained biases in the Doppler signal, we introduced empirical accelerations into the gravitational model. This method offers a flexible way to fit the time-variable components of Jupiter's gravity field without requiring a specific physical model of the normal modes. In this approach, each arc is divided into three segments: the first and last segments exclude empirical acceleration, while the middle 2 hr segment includes it, with a nominal value set to zero in the RTN frame, considering only constant accelerations. These empirical accelerations are updated every 12 minutes with an a priori uncertainty of $5 \times 10^{-8}\,\mathrm{m\,s^{-2}}$ (see Table 3). This segmentation allows for adjustments that better match the observed data, thereby reducing biases and improving the robustness of gravity field estimations. Furthermore, the model incorporates computations for solar radiation pressure on the spacecraft and the dynamics of Jupiter, ensuring a more accurate representation of the forces acting on Juno and Tianwen-4. This comprehensive approach provides a solid foundation for understanding their trajectories and the gravitational dynamics at play.

3.4. Explanation of the Solved-for Parameters

In our estimation filter, we carefully configure both global and arc-wise parameters to ensure accurate modeling and analysis. The specifics of these configurations are detailed in Table 3. This comprehensive approach allows us to maintain consistency across different data segments while addressing the unique characteristics of each arc.

Furthermore, we solved for the Love numbers k_{22}, k_{31}, k_{33}, k_{42}, and k_{44}, which describe Jupiter's tidal response to gravitational forces raised by its moons Io, Europa, Ganymede, and Callisto. Tidal disturbances from Amalthea, Adrastea, Metis, Thebe, and the Sun were excluded, as their tidal parameters are significantly lower than those of Callisto. Specifically, k_{22} was estimated individually for each Galilean moon, while the combined effect of all moons was considered for k_{31}, k_{33}, and k_{42}. This approach was chosen to balance the desire for detailed tidal response information with the need to avoid overparameterization and maintain statistical stability in

Table 3
Description of Estimated Parameters

Parameters	Estimation	A Priori Constraint
Jupiter		
Gravitational parameter μ	Global	none
Tesseral gravity coefficients (C_{21}, S_{21}, C_{22}, S_{22})	Global	none
Zonal gravity coefficients (J_2 to J_{40})	Global	Juno (J_{13} to J_{40}), (Y. Kaspi et al. 2023)
Rotation rate	Global	none
Pole position (Right ascension & decl.)	Global	none
Tidal Love number k_{22} (Io, Europa, Ganymede, Callisto)	Global	Juno, (D. Durante et al. 2020)
Tidal Love numbers k_{31}, k_{33}, k_{42}, k_{44} combined effect of all moons	Global	Juno, (D. Durante et al. 2020)
Spacecraft		
Initial state	Arc-wise	1 km (position), 0.1 m s^{-1} (velocity)
Empirical acceleration	Arc-wise	5×10^{-8} m s^{-2}
Radiation pressure coefficient	Arc-wise	none

the model. By estimating k_{22} separately for each moon, we aimed to capture individual tidal responses, while the combined estimation for higher-order Love numbers allowed us to assess overall tidal effects without risking model instability. The values of the k_{nm} with odd $n - m$ are not observable because the orbits of the satellites of Jupiter have small inclinations. The values for the k_{n0} were fixed to the model predictions because they are not observable given the large correlation with the J_n. The same Love number is imposed for all the satellites.

In our approach, we chose not to impose an a priori constraint on the gravity field coefficients for J_2 to J_{12}, allowing these parameters to remain flexible. The data provided by Juno is sufficiently precise to resolve them and accurately capture the broad, large-scale structure of Jupiter's gravitational field without the need for additional constraints. However, for the coefficients from J_{13} to J_{40}, we applied a priori constraints to manage the challenges posed by the spacecraft's limited sensitivity near the poles. We used the formal uncertainties associated with the zonal harmonics (see Table 3) as the a priori constraints, and we applied values loosened to two times the previously calculated uncertainties, rather than using the exact values.

4. Results

This study utilized simulated tracking data for both the Juno mission and the proposed Tianwen-4 mission. As discussed in Section 3.1, the simulation considered two different orbital inclinations for Tianwen-4, 90° and 40°, and each inclination was tested with two data sets spanning 12 months and 24 months.

4.1. Jupiter Gravity Field Solution

The labels in Figures 4–6 represent the formal uncertainty results derived from analyses of Jupiter's gravity field, based on different data sources and methodologies. The Reference Model refers to the established Jupiter gravity field as resolved by Y. Kaspi et al. (2023), serving as a reference for comparing other models. The estimated Juno model is entirely derived from our simulations based solely on tracking information collected from the Juno mission, replicating the method used to model Jupiter's gravity field with data from this specific mission. Lastly, the Combined Model integrates the tracking data from the Juno mission with additional data anticipated from a proposed future Chinese Tianwen-4 mission to Jupiter. This integration aims to enhance the model's accuracy by combining data from different sources, potentially improving our understanding of Jupiter's gravity field.

We chose the combined solution approach rather than using the Juno solution as an a priori uncertainty for estimating only with Tianwen-4 data because it allows us to integrate and leverage the strengths of each data set and method directly. This approach facilitates a more comprehensive comparison of the potential improvements brought by the additional data from Tianwen-4. Using the Juno solution alone as an a priori uncertainty does not allow us to account for the correlations in parameters between the Juno-derived solution and the Tianwen-4 solution. By employing the combined technique, we can account for these correlations, providing a clearer assessment of the potential contributions of the future Tianwen-4 mission to the accuracy and reliability of Jupiter's gravity field representation.

We conducted a comparison of the formal errors across the reference model, the estimated Juno model from Juno data, and the combined model based on mixed data. The consistency observed between the formal errors of the estimated Juno model and reference model underscores the reliability of our solution, demonstrating the effectiveness of integrating data from multiple missions to refine our knowledge of Jupiter's gravity field.

Figure 4 provides a visualization of the reference zonal harmonics J_n along with a detailed comparative analysis of the formal errors (σ) observed in the gravity field solutions. This figure specifically examines the uncertainties of the solutions derived from the reference model and those obtained using the estimated Juno model, both with and without the inclusion of empirical accelerations. By highlighting these variations, the figure offers valuable insights into the impact of empirical accelerations on the accuracy and reliability of the gravity field solutions, underscoring the importance of their consideration in modeling efforts.

Figure 4 panel (a) represents the reference model of Jupiter's gravity field zonal harmonics J_n with formal uncertainties. Due to the high variation in the first nine values of J_n, the axis is split: the left axis displays the first nine zonal harmonic values on a 10^3 scale, while the right axis represents the remaining values on a 10^7 scale.

Figure 4 panel (b) represents the formal errors on a logarithmic scale to better visualize the differences, illustrating the consistency between the formal errors of the estimated Juno model and the reference model. This underscores the reliability

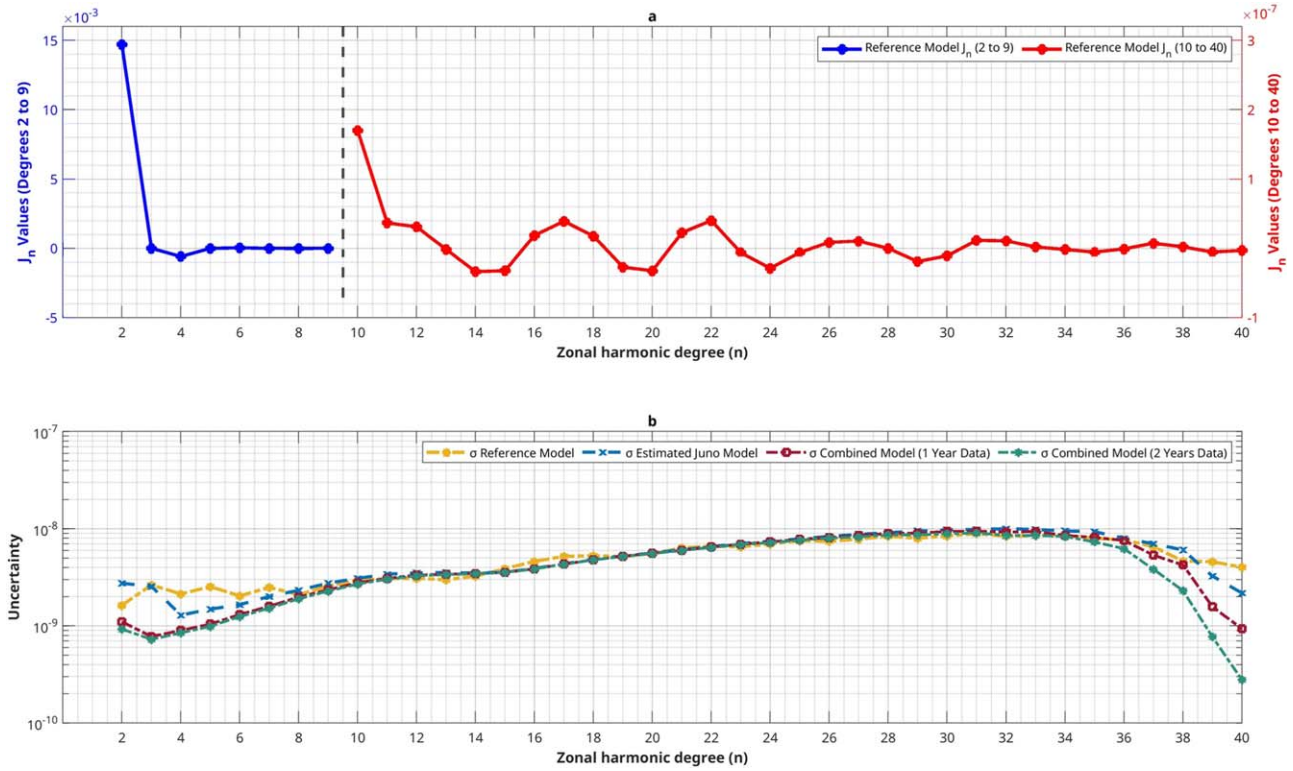

Figure 5. Formal uncertainties (σ) for the gravity field based on a 40° inclination, 12 month and 24 month Tianwen-4 orbit data. Panel (a) displays the zonal harmonics J_n, while panel (b) presents a comparative analysis of these formal uncertainties on a logarithmic scale.
(The data used to create this figure are available in the online article.)

of the uncertainty in our simulated gravity field solution. Empirical accelerations were incorporated into the model to achieve a closer fit to the data, resulting in a noticeable reduction in error magnitude, especially at lower degrees. This analysis highlights the significant effect of empirical accelerations in reducing formal errors at lower degrees, thereby enhancing the alignment with the reference model.

We also plot the a priori values of the coefficients used in the determination of the solutions. While the lower-degree coefficients remain unconstrained, the a priori constraints are applied from J_{13} to J_{40}, as shown in the figure. The results show that the low-degree coefficients are consistent with values reported in the literature.

To further evaluate the impact of empirical accelerations, we also assessed the model without this parameter. The results indicate that with empirical accelerations, the error is higher at lower degrees, with the difference gradually diminishing until degree 15. Beyond degree 15, the error lines of both models converge, showing an overlap that suggests similar performance at higher degrees. This demonstrates the importance of empirical accelerations in improving model realism, especially in the lower-degree components of the gravity field.

The slight difference in formal errors between the reference model and the estimated Juno model, with an average absolute difference of 1.54×10^{-9}, can be explained by a few important factors related to the data and methodologies used in each model. The estimated Juno model relies on simulated data based on initial conditions, which can lead to an underestimation of formal errors. Simulated data often do not fully capture the range of uncertainties and variability found in real observational data. Real data, unlike simulations, can include a variety of unpredictable elements such as instrumental noise, environmental effects, and other anomalies that are difficult to replicate accurately. Additionally, the differences are most pronounced at higher degrees and are primarily influenced by the a priori constraints.

The influence of the Tianwen-4 orbital configuration across spherical harmonic degrees is evaluated over 12 and 24 month data collection periods. Figure 5 depicts results for a 40° orbit, while Figure 6 shows results for a 90° polar orbit.

Figure 5 illustrates the formal errors associated with the gravity field harmonics for both 12 month and 24 month data collection periods at a 40° orbital inclination. The results show that the formal errors in the combined model closely mirror those of the Juno estimated model across most observed degrees, except for the first six and last four degrees. Extending the data duration to 24 months does not significantly enhance the accuracy for lower-degree harmonics, showing only minor precision improvements compared to the 12 month scenario. This suggests that simply increasing the mission duration may not always yield proportional improvements in gravity field estimations, particularly for the fundamental harmonics, and highlights potential trade-offs between mission duration, data quality, and modeling complexity. The limited global coverage from a 40° orbit significantly hinders its ability to make a competitive contribution to our understanding of Jupiter's gravity field.

Figure 6 examines the formal errors associated with the spherical harmonic coefficients for 90° inclination orbits using 12 month and 24 month data collection periods. The 12 month data demonstrate significant enhancements in measurement accuracy up to degree 20, after which the errors converge with those observed in the estimated Juno model. This highlights the effectiveness of high-inclination orbits in capturing detailed

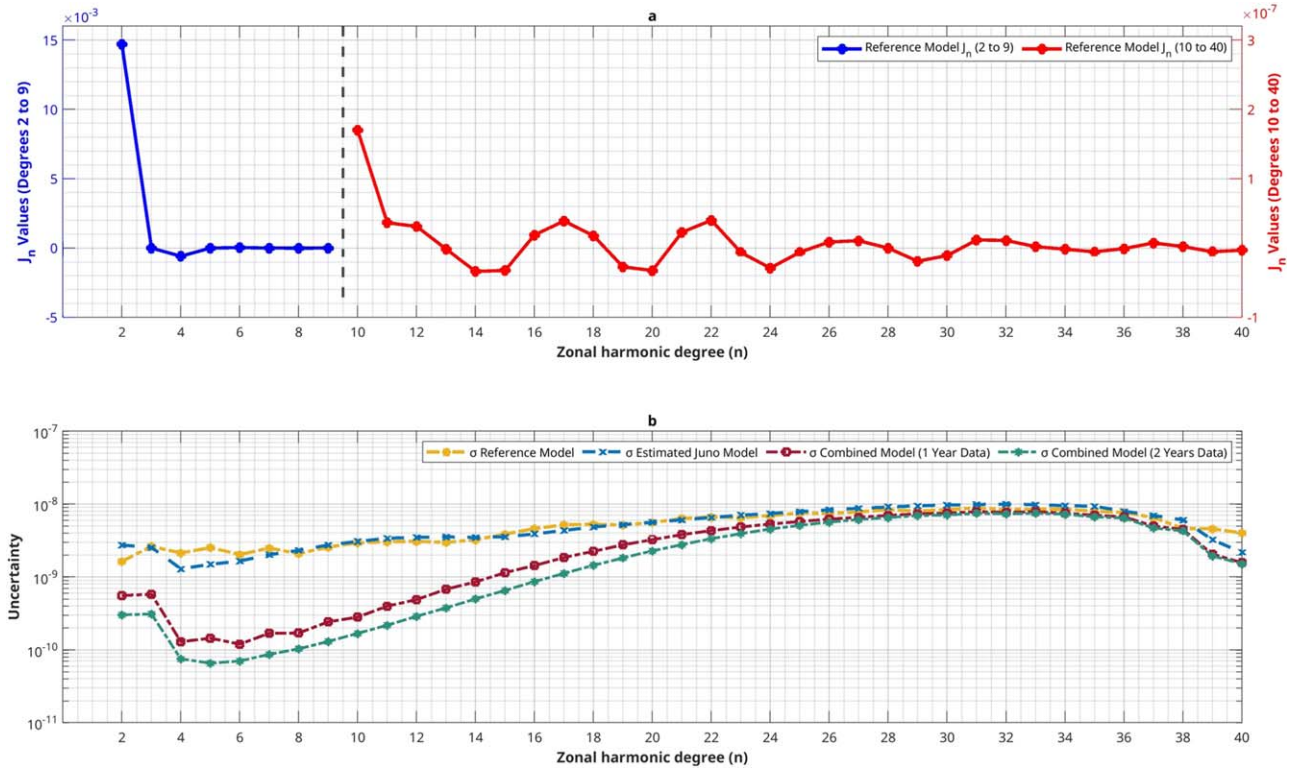

Figure 6. Formal uncertainties (σ) for the gravity field based on a 90° inclination, 12 month and 24 month Tianwen-4 orbit data. Panel (a) displays the zonal harmonics J_n, while panel (b) presents a comparative analysis of these formal uncertainties on a logarithmic scale.
(The data used to create this figure are available in the online article.)

gravitational anomalies that are less perceptible in lower-inclination orbits. The 24 month data further reduces the formal errors; this indicates that the coefficients are well determined and reliable, with formal errors comparable to those observed in a shorter, 12 month data collection period. The similarity in error magnitude despite the extended duration highlights the efficiency of data utilization over longer observational periods at this inclination.

The results presented in Figures 4 through 6 demonstrate the substantial impact of various inclination angles and data durations from the Tianwen-4 mission on the estimation of the gravity field. The detailed examination across these figures highlights the precision with which spherical harmonic coefficients can be determined when leveraging longer data sets and varying inclinations. While some degrees show minimal improvement, the overall accuracy and formal error enhancements highlight the effectiveness of incorporating extended and diverse observational data. For the 90° inclination with 24 months of data, the average improvement factor is 20.08 for degrees 2–12, gradually decreasing to an average factor of 2.46 for higher degrees, with an overall accuracy improvement factor of 7.43. In contrast, for the 40° inclination with 24 months of data, the overall average improvement factor is 1.73. This comprehensive approach sets a firm foundation for future explorations and studies of Jupiter's complex gravitational environment.

4.2. Tidal Effects

In our analysis, we adopted reference Love number values as provided in (D. Durante et al. 2020). These values serve as the baseline for our comparative analysis of estimated Love numbers. To validate our solution, we ran computations for the Estimated Juno model using an a priori covariance set to 5 times the value of the previously calculated uncertainty, which represents a very loose constraint. This analysis focuses on the separate effect of the Love number k_{22} and the combined influence of higher-order Love numbers. The results of this comparison are presented in Figure 7, which shows both the reference model formal errors and the Estimated Juno model formal errors, each displayed with 1σ uncertainty.

Figure 7 shows the separate effect of the uncertainty of satellite-dependent Love number k_{22} for Io, Europa, Ganymede, and Callisto, alongside the combined influence of higher-order Love numbers (k_{31}, k_{33}, k_{42}, k_{44}). For the comparison, the reference formal error values for k_{22} (Io) and the higher-order Love numbers are taken from D. Durante et al. (2020) based on real data. However, because D. Durante et al. (2020) do not provide satellite-dependent values for k_{22} for Europa, Ganymede, and Callisto, we have sourced these values from V. Notaro et al. (2019), a simulation study. The reference model shows lower uncertainties for k_{22} for Europa, Ganymede, and Callisto compared to the estimated Juno model, likely due to differences in methodology, as V. Notaro et al. (2019) focused on tidal response rather than gravity field estimations. In addition, our analysis differs in duration and number of arcs, using a 7 hr arc length instead of 48 hr, and 26 arcs instead of 22.

For k_{22} (Io) and higher-order Love numbers with the combined effect from all moons, the estimated Juno model follows the same trend as the reference formal errors, though with slightly lower uncertainties compared to the reference Juno model. The lower uncertainty in the k_{22} (Io) and higher-order Love numbers is possibly due to the number of arcs used.

We used 26 arcs to clone the gravity field model derived by Y. Kaspi et al. (2023). Since Y. Kaspi et al. (2023) were not

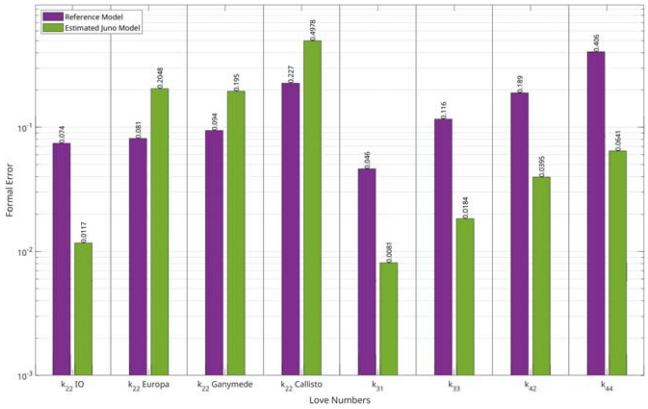

Figure 7. Formal error comparison of separate Love number k_{22} and combined higher-order Love numbers for Jupiter's Galilean moons. Note that the "reference Juno model" values for k_{22} (Europa, Ganymede, and Callisto) are taken from V. Notaro et al. (2019), which uses different settings than the rest of the model from D. Durante et al. (2020).

(The data used to create this figure are available in the online article.)

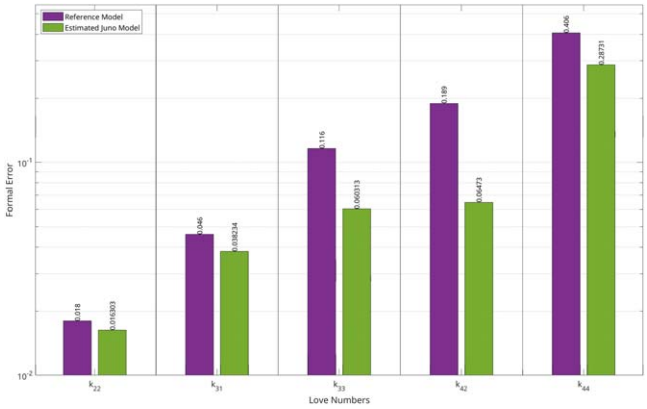

Figure 8. Jupiter's static Love numbers k_{22}, k_{31}, k_{33}, k_{42}, and k_{44} formal uncertainties, representing the combined effect of all Galilean moons, for the estimated Juno model (midmission data set) and the reference Juno model.

(The data used to create this figure are available in the online article.)

primarily focused on tidal estimation, we opted to use the previous Love number data. To further validate k_{22} and the higher-order Love numbers, we adjusted our simulation to 10 arcs, as estimated by D. Durante et al. (2020), where k_{22} is considered a combined effect of all satellites.

Figure 8 shows that the formal errors in k_{22} with the combined effect closely align with the reference value, validating our solution. Additionally, our higher-order Love numbers also align closely with the reference values; however, some deviations still exist. This highlights that certain model differences remain, despite the overall good alignment. The increase in arcs from 10 to 26 explains why the uncertainties in our analysis are lower than those in the reference Juno model for higher-order Love numbers (D. Durante et al. 2020).

Building on this, Figures 9 and 10 illustrate the 3σ formal uncertainties of Jupiter's static k_{22} and higher-order Love numbers k_{31}, k_{33}, k_{42}, and k_{44}. Due to some of the values being very small, Table 4 provides a detailed comparison of these uncertainties under orbital inclinations of 40° and 90° and data collection durations of 1 yr and 2 yr for both the combined model and the estimated Juno model.

Figure 9 illustrates a color-coded graph representing 40° and 90° orbital inclinations and data collection durations of 1 yr and 2 yr for the combined model, as well as the estimated Juno model. This figure provides a detailed comparison of the formal uncertainties between the estimated Juno and combined values for Jupiter's tidal Love number (k_{22}), highlighting the potential enhancements achieved with the incorporation of Tianwen-4 mission data. Notably, the results show significant refinement in k_{22} estimates for the 40° inclination orbit with 24 months of data collection. These improvements in k_{22} precision are crucial for enhancing our understanding of Jupiter's internal tidal response to the gravitational forces exerted by its moons. A particularly promising result is that, with the Tianwen-4 data, frequency-dependent k_{22} values (at Io, Europa, and Ganymede frequencies) can be properly constrained at the 3σ level, something that was not achievable with Juno data alone (V. Notaro et al. 2019).

Figure 10 illustrates the formal uncertainties for the Love numbers k_{31}, k_{33}, k_{42}, and k_{44}. The graph is color coded to represent different orbital inclinations and data collection durations. We observed modest improvements in the precision

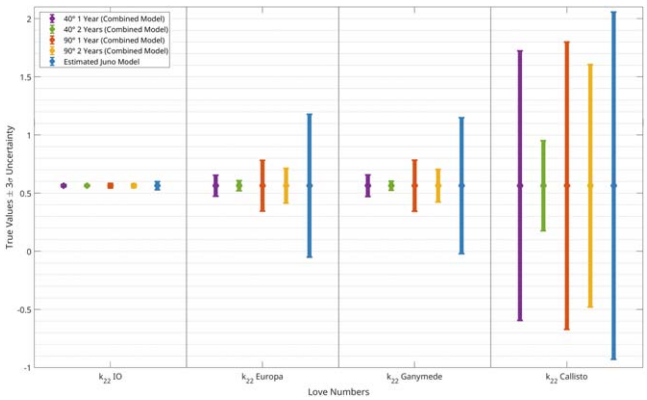

Figure 9. Jupiter's satellite-dependent static Love numbers (dots) k_{22} with 3σ formal uncertainties for each Galilean moon (Io, Europa, Ganymede, and Callisto) under different orbital inclinations and data collection durations for the combined model, as well as the estimated Juno model. Please see Table 4 for the numerical values.

(The data used to create this figure are available in the online article.)

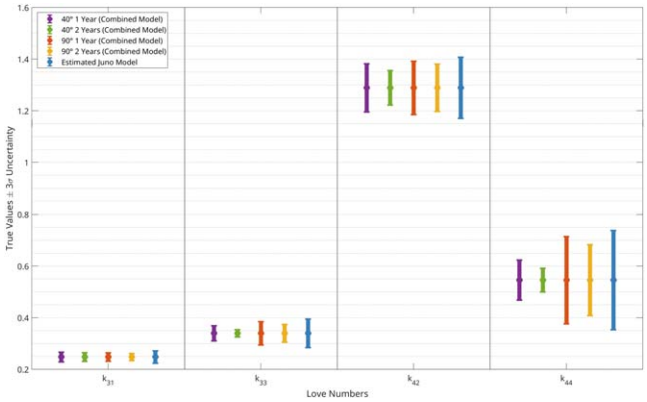

Figure 10. Jupiter's static Love numbers (dots) k_{31}, k_{33}, k_{42}, and k_{44} with 3σ formal uncertainties, representing the combined effect of all Galilean moons, under different orbital inclinations (40° and 90°) and data collection durations (1 yr and 2 yr) for the combined model, as well as the estimated Juno model. Please see Table 4 for the numerical values.

(The data used to create this figure are available in the online article.)

of Love numbers k_{33}, k_{42}, and k_{44} for the 40° inclination orbit with 24 months of data collection. Interestingly, Love numbers k_{31} show better precision for the 90° inclination orbit, also with

Table 4
Jupiter's Static k_{22} (Satellite-dependent) and Higher-order (Combined Effect) Love Number's 3σ Uncertainties, under Different Orbital Inclinations (40° and 90°) and Durations (1 yr and 2 yr), for Combined and the Estimated Juno Models

	Estimated Combined Models				Estimated Juno Model
	40°, 1 yr	40°, 2 yr	90°, 1 yr	90°, 2 yr	
k_{22} IO	0.011675	0.006074	0.019955	0.016528	0.035145
k_{22} Europa	0.089830	0.043835	0.217738	0.149262	0.614319
k_{22} Ganymede	0.093247	0.039593	0.219721	0.140488	0.585081
k_{22} Callisto	1.159051	0.387210	1.236153	1.043160	1.493481
k_{31}	0.018789	0.016817	0.016347	0.013406	0.024167
k_{33}	0.029335	0.014168	0.044939	0.034425	0.055318
k_{42}	0.093113	0.066756	0.103253	0.091530	0.118418
k_{44}	0.077423	0.045611	0.168896	0.137413	0.192202

24 months of data. These results highlight the complex relationship between orbital parameters, mission duration, and the precision of Love number estimations, as different inclinations and timeframes affect the spacecraft's sensitivity to gravitational forces, influencing Love number precision.

The reduced formal errors observed for k_{22}, k_{33}, k_{42}, and k_{44} at an inclination of 40° are due to the increased sensitivity of these Love numbers to the low- and mid-latitude regions where Jupiter's gravitational potential varies most significantly, as depicted in Figure 1. In this orbit, the spacecraft revisits these regions more frequently, allowing for a more precise sampling of gravitational forces from Jupiter's moons and the planet's higher-order gravitational harmonics. As a result, the differences in the measured gravitational field provide valuable data for estimating these Love numbers, leading to significantly improved precision compared to the 90° orbit, as shown in Figure 2.

For k_{31} and k_{42}, which are more dependent on the global distribution of mass, the polar trajectory at 90° inclination continues to provide better constraints. However, the differences in formal uncertainties for k_{31} and k_{42} between the two inclinations are relatively small compared to the larger improvements seen for k_{22}, k_{33}, and k_{44} at 40°. This suggests that while the polar orbit enhances global gravitational coverage, the 40° orbit still provides competitive results for most Love numbers (see Table 4). Additionally, Love numbers such as k_{20} and k_{30}, which are influenced by lower-order terms, remain fixed to model predictions due to their large correlation with the J_n (zonal harmonics), making them less sensitive to variations sampled at either inclination.

4.3. Correlation of Gravity Field Coefficients and Love Numbers

The series of correlation diagrams presented in Figures 11, 12, and 13 elucidate the effect of different data integration strategies on the cross-correlations among solved parameters in Jupiter's gravitational model. These figures illustrate how the integration of additional data affects the decorrelation of gravity coefficients from rotational parameters, a crucial aspect for enhancing the precision and reliability of the gravitational model.

Figure 11 displays the correlation matrix derived solely from the Juno mission's estimated solution. Here, significant off-diagonal cross-correlations are observable among the parameters, including the constant rotation rate ω, R.A. α, decl. δ, k_{22} (individual), k_{31}, k_{33}, k_{42}, and k_{44} (combined) Love numbers, and gravitational coefficients such as C_{20}, C_{21}, C_{22}, and C_{30} to C_{40}, as well as S_{21} and S_{22}. The low correlation of the degree-2 tesseral coefficients with other terms is primarily due to their dependence on the rotational parameters of the body. Tesseral coefficients, which describe the nonaxisymmetric components of a planet's gravity field, are sensitive to the planet's rotation and shape. In particular, the observed correlations can be influenced by the planet's rotational dynamics, as these coefficients are closely tied to the planet's equatorial bulge and rotational deformation. Additionally, the observational geometry and data coverage, especially in equatorial regions, further limit the sensitivity of measurements to these coefficients. These correlations indicate dependencies that can complicate the interpretation and accuracy of gravitational data.

Figure 12 shifts to a scenario where data from the Tianwen-4 mission, collected at a 40° inclination over 24 months, is integrated with Juno data. This configuration shows a minor reduction in cross-correlations, particularly between the Love numbers and the gravitational coefficients. This improvement is attributed to the increased geometric coverage and diverse observational angles provided by the combined data set, which helps in effectively separating the influence of rotational dynamics from the gravitational coefficients.

Figure 13 explores the correlations when using data from a 90° inclination over the same 24 month period. The diagram here further demonstrates a reduction in cross-correlations, even more pronounced than in the 40° case. This setup provides the most comprehensive spatial coverage, particularly enhancing the decorrelation of parameters that are sensitive to polar observational geometries. The increase in correlations for high-degree coefficients can be attributed to the reduced influence of a priori constraints at higher degrees. This allows the data collected during the mission to have a greater impact on determining these coefficients. While recent work by G. Lari et al. (2024) has effectively decorrelated the gravity coefficients by employing a comprehensive rotational dynamics model for Jupiter, our model is not as extensive in

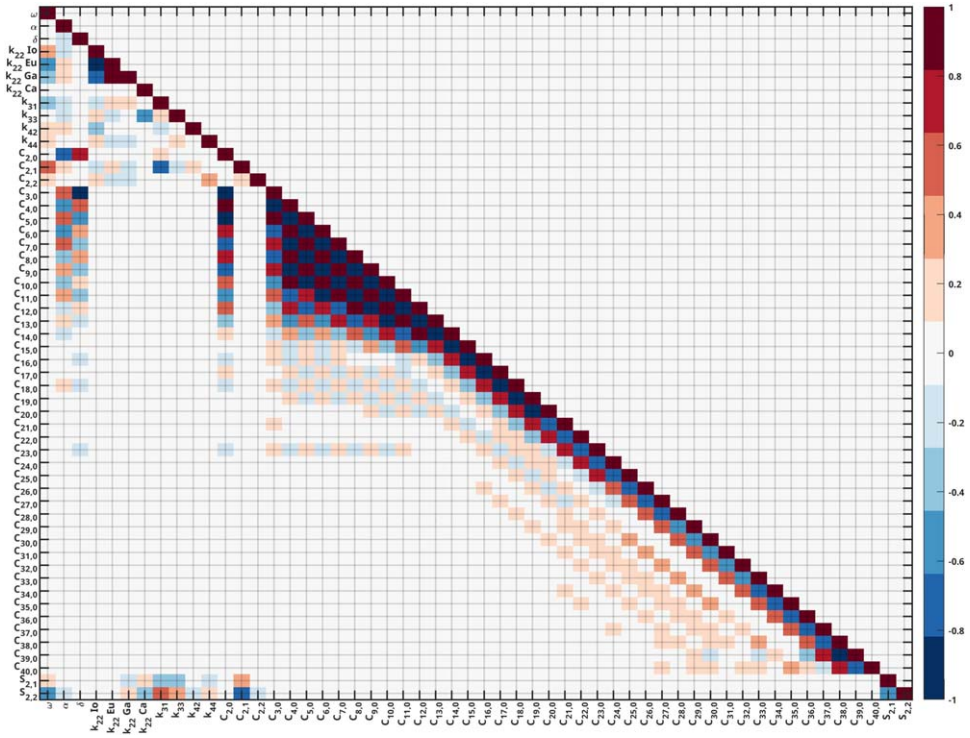

Figure 11. Depiction of the normalized correlation coefficients between gravity field and Love numbers, along with rotational parameters, for the estimated Juno model.

(The data used to create this figure are available in the online article.)

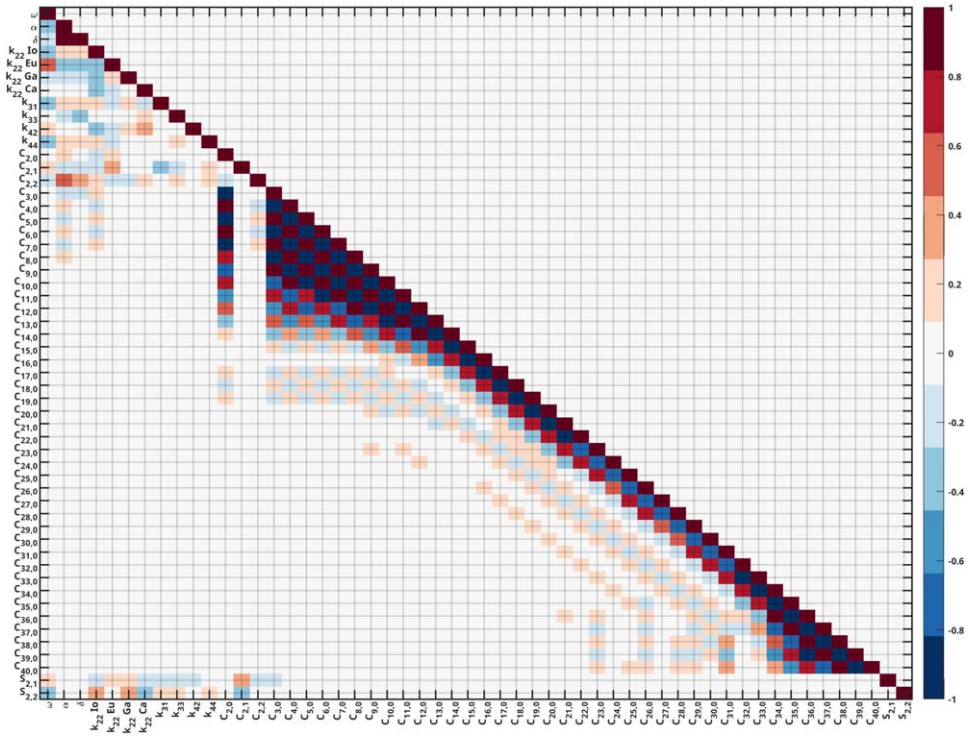

Figure 12. Depiction of the normalized correlation coefficients between gravity field and Love numbers, along with rotational parameters, for a 40° inclination over 24 months.

(The data used to create this figure are available in the online article.)

terms of rotational dynamics. However, by combining Juno data with Tianwen-4 data, our analysis provides unique advantages. Tianwen-4 provides complementary observational geometries that Juno alone cannot achieve, further enhancing the precision and reliability of our gravitational model for Jupiter.

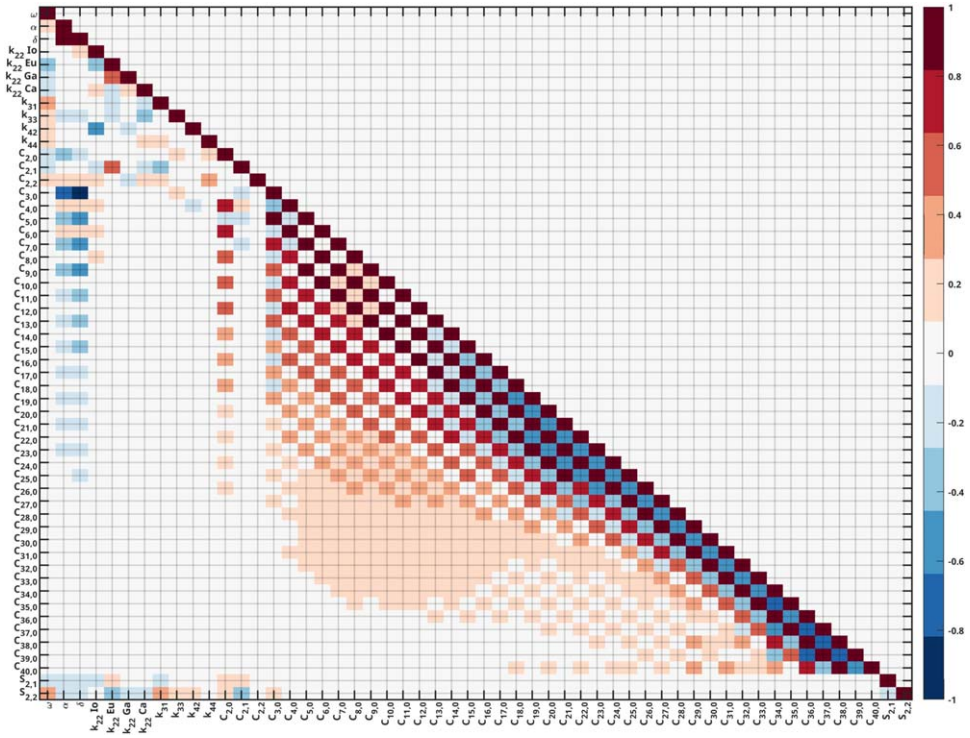

Figure 13. Depiction of the normalized correlation coefficients between gravity field and Love numbers, along with rotational parameters, for a 90° inclination over 24 months.

(The data used to create this figure are available in the online article.)

5. Discussion and Conclusions

This research has provided a detailed error analysis of Jupiter's gravity field for future missions by determining formal uncertainties through a combination of simulated data from Juno and the anticipated Tianwen-4 mission. These efforts provide us with a better quantitative understanding of the influence of orbital dynamics, particularly inclination and the duration of data collection, in accurately capturing the gravitational nuances and tidal effects on Jupiter.

The choice of 90° and 40° inclinations for the orbits in our simulations has proved critical in extending the spatial coverage of gravitational measurements across a broader range of latitudes (see Figure 2 for satellite ground tracks at 90°). Higher inclinations enhance the detection and refinement of spherical harmonic coefficients by improving sampling in latitudinal directions that are less explored by lower-inclination orbits (as shown in Figures 5 and 6 for gravity field coefficients). This increased coverage leads to substantial improvements in the precision of the gravity field models, with accuracy improving by a factor of up to 20.02 in the first 12°, decreasing to an average factor of 2.46, and resulting in an overall averaged enhancement factor of 7.43 (see Figures 6 for details). This is particularly crucial for observing the asymmetric components of Jupiter's gravity field, which are influenced by dynamic atmospheric phenomena and the massive cyclones at the poles.

Conversely, the choice of a 40° inclination has been particularly beneficial for determining tidal responses, better capturing the tidal bulges induced by Jupiter's moons. This inclination provides a balance between observing equatorial regions and accessing significant latitudinal coverage up to mid-latitudes, which is crucial for a comprehensive view of tidal effects without the need for extensive polar observations. While the precision in gravitational field coefficients at this inclination may not be as high for all Love numbers, the reduced uncertainties for k_{22}, k_{33}, k_{42}, and k_{44} significantly improve the potential scientific outcomes of the mission, with an average overall improvement factor of 6.90 compared to estimated Juno model. Conversely, the 90° inclination provides better constraints on k_{31} with improved uncertainties and an enhancement factor of 1.80 due to the enhanced sensitivity to higher-order terms in the gravitational potential (see Figures 9 and 10 for details). These simulations are beneficial for future missions, as they provide valuable insights into how such missions can gather data to improve our understanding of Jupiter's internal structure and dynamics.

Furthermore, the lengthened data collection periods, as examined with the 24 month data set, afford a more detailed observation of the temporal variations within the gravitational field. This amount of temporal data is essential for diminishing correlations between zonal harmonics, thereby increasing the resolution and precision of the gravitational model (see Figures 12 and 13 for correlation images). Extended observation periods enhance the precision of gravitational field estimations by reducing correlations among parameters, thereby improving the stability and accuracy of Jupiter's gravitational model.

In relation to earlier studies, our work builds upon the significant contributions of D. Durante et al. (2020), Y. Kaspi et al. (2023), G. Lari et al. (2024), V. Notaro et al. (2019), and M. Parisi et al. (2021), who have provided fundamental insights into Jupiter's gravity field, tidal dynamics, and the internal structure of its moons. In our study, we have expanded on this foundation by integrating simulated data from the Juno and anticipated Tianwen-4 missions to further refine our models.

These multimission data simulations offer a more comprehensive understanding of Jupiter's gravitational environment, building upon and extending the capabilities explored in previous missions.

In a broader context, our work aligns with ongoing multimission data analysis efforts within the Jovian system, particularly involving the JUICE and Europa Clipper missions. The joint analysis of tracking data from these missions, as explored by M. Fayolle et al. (2024), illustrates the role PRIDE very long baseline interferometry (VLBI) products play in improving the determination of ephemerides for Jupiter's moons, especially during critical flybys where local state solutions are essential. Similarly, A. Magnanini et al. (2024) emphasize the potential of combining radio science data from JUICE and Europa Clipper to deepen our understanding of tidal dissipation and the dynamic coupling between Jupiter and its moons. Moreover, the integration of astrometry and radio science from these missions, as discussed by M. Fayolle et al. (2023), enhances the accuracy of Galilean moon ephemerides by combining short-term mission data with long-term astrometric records. These collaborative efforts exemplify the growing importance of integrating diverse data sets from multiple missions, which could further enrich our understanding of Jupiter's gravitational field and tidal interactions beyond what single-mission data sets, such as those from Juno or Tianwen-4, can achieve.

The concurrent operations of JUICE, Europa Clipper, and Tianwen-4 in the Jovian system present a unique opportunity to globally estimate the gravitational fields of Jupiter and its moons, with all coupling effects consistently accounted for. By integrating data sets from these missions, it becomes possible to create a more complete model of the system's gravity fields. JUICE's geophysical characterization of Ganymede, Callisto, and Europa provides crucial insights into the internal structures of these moons (T. Van Hoolst et al. 2024). This involves combining multiple data types, including gravity, topography, magnetic field measurements, and radar soundings, which together offer a more comprehensive understanding of their interiors. When further refined by Europa Clipper's focus on Europa's ice shell and potential subsurface ocean, these data sets significantly improve our models. Complementing these efforts, Tianwen-4 contributes to a more detailed understanding of Jupiter's gravity field, enabling a complete representation of tidal dissipation and dynamic coupling between Jupiter and its moons. Together, these missions create a multimission synergy that enhances our ability to model the Jovian system and provides a more accurate understanding of the gravitational interactions within this system.

The future determination of Jovian ephemerides will be substantially enhanced by data integration from multiple missions. While Juno and JUICE contribute through their range data, refining the precision of orbital parameters, the use of VLBI data—such as that gathered from Juno's astrometric observations (D. L. Jones et al. 2019)—further sharpens the accuracy of these measurements. The PRIDE experiment on JUICE (L. I. Gurvits et al. 2023) will provide additional high-precision measurements that can be used to complement the foundational ephemerides established in the DE440 and DE441 models (R. S. Park et al. 2021). These efforts from multiple missions will enable a more nuanced understanding of the Jovian system, its gravitational interactions, and the orbital evolution of its moons.

Our study reveals significant improvements in the determination (and modeling the interior) of Jupiter's gravitational field through the integration of Juno data with simulated Tianwen-4 mission data. The 90° orbital inclination plays a crucial role in enhancing the precision of gravitational coefficients and tidal estimations, offering comprehensive coverage of Jupiter's poles and refining the precision of gravitational coefficients, with improved uncertainty estimates up to degree 40. In contrast, the Tianwen-4 spacecraft with an inclination of 40° proves particularly effective for estimating Love numbers such as k_{22}, k_{33}, and k_{44}, capturing tidal bulges and providing better constraints on Jupiter's internal structure. Additionally, extended data collection periods further enhance uncertainty estimates, leading to more accurate models. These advancements contribute to a deeper understanding of Jupiter's internal dynamics and help advance theoretical models in planetary science, which are essential for informing future exploratory missions.

Acknowledgments

We appreciated the hard work of the Juno mission and Tianwen-4 mission that made this research possible. J.Y. is supported by a grant provided by the National Key Research and Development Program of China (No. 2022YFF0503202), the National Natural Science Foundation of China (Nos. 42241116, 42402230), and the 2022 Project of Xinjiang Uygur Autonomous Region of China for Heaven Lake Talent Program. Z.W. is supported by the Chinese Academy of Sciences Foundation of the young scholars of western (2020-XBQNXZ-019) and the open project of the Key Laboratory in Xinjiang Uygur Autonomous Region of China (2023D04058).

ORCID iDs

Zohaib Afzal https://orcid.org/0009-0006-1279-9245
Jianguo Yan https://orcid.org/0000-0003-2612-4776
Dominic Dirkx https://orcid.org/0000-0003-2069-0603
Zhen Wang https://orcid.org/0000-0002-3849-6692
Jean-Pierre Barriot https://orcid.org/0000-0002-2112-9685

References

Acton, C. H., et al. 1996, P&SS, 44, 65
Asmar, S. W., Bolton, S. J., Buccino, D. R., et al. 2017, SSRv, 213, 205
Bauer, S., Hussmann, H., Oberst, J., et al. 2016, P&SS, 129, 32
Bertotti, B., Ferinella, P., & Vokrouhlický, D. 2003, Physics of the Solar System: Dynamics and Evolution, Space Physics and Spacetime Structure, 293 (Dordrecht: Kluwer)
Bolton, S. J., Levin, S. M., Guillot, T., et al. 2021, Sci, 374, 968
Bolton, S. J., Lunine, J., Stevenson, D., et al. 2017, SSRv, 213, 5
Dirkx, D., Mooij, E., & Root, B. 2019, Ap&SS, 364, 37
Dirkx, D., Fayolle, M., Garrett, G., et al. 2022, in Europlanet Science Congress 2022, 16
Durante, D., Guillot, T., Iess, L., et al. 2022, NatCo, 13, 4632
Durante, D., Parisi, M., Serra, D., et al. 2020, GeoRL, 47, e86572
Fayolle, M., Dirkx, D., Cimo, G., et al. 2024, Icar, 416, 116101
Fayolle, M., Lainey, V., Dirkx, D., et al. 2023, A&A, 676, L6
Folkner, W. M., Iess, L., Anderson, J. D., et al. 2017, GeoRL, 44, 4694
Fuller, J., Luan, J., & Quataert, E. 2016, MNRAS, 458, 3867
Guillot, T. 1999, Sci, 286, 72
Guillot, T., Miguel, Y., Militzer, B., et al. 2018, Natur, 555, 227
Guillot, T., Stevenson, D. J., Hubbard, W. B., & Saumon, D. 2004, in Jupiter: The Planet, Satellites and Magnetosphere, ed. F. Bagenal, T. E. Dowling, & W. B. McKinnon (Cambridge: Cambridge Univ. Press)
Gurvits, L. I., Cimò, G., Dirkx, D., et al. 2023, SSRv, 219, 79
Hubbard, W. B. 1999, Icar, 137, 357
Iess, L., Folkner, W. M., Durante, D., et al. 2018, Natur, 555, 220

Jones, D. L., Romney, J. D., Folkner, W. M., et al. 2019, in 2019 IEEE Aerospace Conf. (Piscataway, NJ: IEEE), 1
Kaspi, Y. 2013, GeoRL, 40, 676
Kaspi, Y., Flierl, G. R., & Showman, A. P. 2009, Icar, 202, 525
Kaspi, Y., Galanti, E., Hubbard, W. B., et al. 2018, Natur, 555, 223
Kaspi, Y., Galanti, E., Park, R. S., et al. 2023, NatAs, 7, 1463
Kaspi, Y., Hubbard, W. B., Showman, A. P., & Flierl, G. R. 2010, GeoRL, 37, L01204
Lari, G., Zannoni, M., Durante, D., Park, R. S., & Tommei, G. 2024, Aeros, 11, 124
Love, A. E. H. 1911, Some Problems of Geodynamics (Cambridge: Cambridge Univ. Press)
Magnanini, A., Zannoni, M., Casajus, L. G., et al. 2024, A&A, 687, A132
Montenbruck, O., Gill, E., & Lutze, F. 2002, ApMRv, 55, B27
Moyer, T. D. 2003, Formulation for Observed and Computed Values of Deep Space Network Data Types for Navigation (New York: Wiley) 10.1002/0471728470
Notaro, V., Durante, D., & Iess, L. 2019, P&SS, 175, 34
Parisi, M., Kaspi, Y., Galanti, E., et al. 2021, Sci, 374, 964
Park, R. S., Folkner, W. M., Williams, J. G., & Boggs, D. H. 2021, AJ, 161, 105
Planetary Atmospheres Node 2024, https://pds-atmospheres.nmsu.edu/
Serra, D., Spoto, F., & Milani, A. 2018, CeMDA, 130, 75
Shangbiao, S., Yan, J., & Liu, S. 2025, ApJ, 979, 221
Slobin, S. D. 2016, 301 Coverage and Geometry 810-005, 301, Rev. K, Jet Propulsion Laboratory, California Institute of Technology, http://deepspace.jpl.nasa.gov/dsndocs/810-005/
Stevenson, D. J. 2020, AREPS, 48, 465
Sun, S., Yan, J., Gao, W., et al. 2024, AJ, 168, 3
Van Hoolst, T., Tobie, G., Vallat, C., et al. 2024, SSRv, 220, 54
Vasavada, A. R., & Showman, A. P. 2005, RPPh, 68, 1935
Wahl, S. M., Hubbard, W. B., & Militzer, B. 2016, ApJ, 831, 14
Wahl, S. M., Hubbard, W. B., & Militzer, B. 2017, Icar, 282, 183
Yan, J., Yang, X., Hao, W., et al. 2017, Ap&SS, 362, 236